MICROCHANNEL HEAT EXCHANGER AIR SIDE HEAT TRANSFER ANALYSIS AND OPTIMIZATION

Glazar, V.*,Trp, A. and Lenic, K.
*Author for correspondence
Department of Thermodynamics and Energy Engineering,
Faculty of Engineering,
University of Rijeka,
Vukovarska 58,
51000 Rijeka,
Croatia,
E-mail: vladimir.glazar@riteh.hr

ABSTRACT

Heat transfer simulations in a heat exchanger with the microchannel coil have been done and described in this paper. The aim of this study was to use a previously validated mathematical model and numerical procedure of compact heat exchangers type with straight microchannels and to investigate heat fluxes dependence on different geometry and operating parameters. According to dimensions of the heat exchanger, which is commonly used in HVAC units as a condensing unit, a 3D mathematical model has been defined and solved numerically. The objective function has been developed with selected input parameters of heat exchanger: fin pitch, flat tube transversal row pitch, and air inlet velocity. Response surface methodology has been applied to derive a polynomial function that describes power density change according to three selected input parameters. Finally, the created function has been subjected to genetic algorithm optimization procedure. Optimal setup for a given geometry and operating parameters has been acquired and followed with discussion and conclusions.

INTRODUCTION

Permanent need for improvement of heat transfer has led to the use of microchannels in compact heat exchangers. In this way, extremely high heat transfer rates can be achieved under confined conditions [1]. Heat exchangers with microchannel coil (further in text MCHX) are widely used in various ways as HVAC unit condensers, evaporators or for water coil applications [2]. Their modular design, high-efficiency heat exchange, and robustness are some of their advantages compared to other types of compact heat exchangers [3]. A large number of research papers about MCHX can be found with different topics that deal with both single phase [4, 5] or with phase change processes [6, 7]. According to [8], the performance of the heat exchanger can be evaluated by various criteria: coefficient of performance (COP), compactness factor (CF) and power density (PD). COP is defined as the ratio of the total heat removed to the electrical input of the blower. CF is the total heat removed per unit of heat exchanger volume and PD is total heat removed per unit of heat exchanger mass.

NOMENCLATURE

Abbreviations	
CF	compactness factor
COP	coefficient of performance
MCHX	heat exchangers with microchannel coil
PD	power density
Special characters	
c	specific heat capacity, J kg^{-1} K^{-1}
d_h	hydraulic diameter, m
F_p	fin pitch, m
F_t	fin thickness, m
k	thermal conductivity, W m^{-1} K^{-1}
m	mass, kg
n	normal direction coordinate, m
p	pressure, Pa
P_t	transversal MCHX tube row pitch, m
R^2	coefficient of determination
Q	heat transfer rate, W
T	temperature, K
u	x-axis velocity component, m s^{-1}
v	y-axis velocity component, m s^{-1}
w	z-axis velocity component, m s^{-1}
$\vec{u}$	velocity vector, m s^{-1}
x, y, z	Cartesian coordinates, m
x	Uncoded input parameter
X	Coded input parameter
Greek	
μ	dynamic viscosity, Pa s
ρ	density, kg m^{-3}
Subscripts	
a	air
f	fin
in	inlet
max	maximum
mc	microchannel
min	minimum
out	outlet
ref	referent
t	tube

In this paper, Response Surface Methodology, combined with Box-Behnken technique [9], has been used to find an air-side parameter setup that best fits the demand of microchannel heat exchanger for maximum power density. This method uses specially designed parameter setup to obtain an optimal response according to the developed objective function. Base dimensions used for the creation of the referent model were taken from the heat exchanger described in [10]. The referent model was the one that had all geometry parameters in the middle of the selected input parameters range.

For the purpose of this investigation, a set of 15 design points with different parameter setups has been created [11]. Two different geometry parameters of the heat exchanger were examined, combined with one operating condition. Previously experimentally validated 3D mathematical model and the numerical procedure was used to predict the heat transfer rate for each of the design points [12]. Heat transfer and fluid flow simulations were performed using fluid flow and a heat transfer solver FLUENT.

Multivariate optimization carried in this paper included fin pitch, transversal MCHX tube row pitch and air inlet velocity as variables, and the objective function with the goal of maximizing the power density of examined heat exchanger. Nonlinear regression model of the objective function for the prescribed data set has been made and appropriate response surface plots have been generated and shown. Finally, the developed function has been subjected to genetic algorithm optimization procedure. Optimal setup for a given geometry and operating parameters have been acquired and followed with discussion and conclusions.

MATHEMATICAL AND NUMERICAL APPROACH

Physical Model

The main dimensions used for modelling of referent MCHX were based on the heat exchanger that was experimentally tested and analysed [10]. Table 1 gives the values of basic geometry parameters.

Table 1 Basic geometry parameters

Geometry parameter	mm
Transversal tube row pitch, P_t	11
Fin pitch, F_p	1
Fin thickness, F_t	0.1
Hydraulic diameter, d_h	1.44

Due to limitations of computer resources and to save computational time, only part of the heat exchanger (one flat tube and one fin), required to describe airflow and heat transfer, was taken as a computational domain. A schematic view of the computational domain has been shown in Figure 1. In the figure, the upstream and downstream regions have not been fully presented.

Two symmetry planes were assumed in the z-direction that divides space between flat tubes into two symmetrical parts (upper and lower symmetry planes). These planes were perpendicular to the fin surface. Additionally, two symmetry planes were assumed in the y-direction on both air and tube subdomains (left and right symmetry planes). The left symmetry plane (not shown in Figure 1) is placed on the opposite side of the right symmetry plane according to fins.

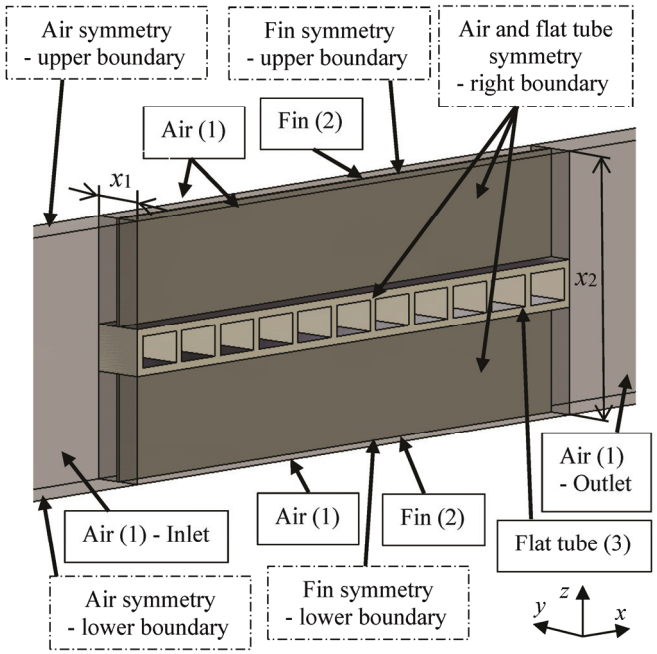

Figure 1 Schematic view of the computational domain

The computational domain consists of three subdomains: air (1), fin (2) and flat tubes (3). The total length of the computational domain has been extended 6.5 times from actual internal airspace. The upstream air region has been extended 1.5 times to ensure the correct inlet velocity profile in near tube and fin region. The downstream air region has been extended 5 times, thus a developed flow pattern at the outlet boundary can be assumed [13]. Reynolds number was in all cases lower than 2000 and flow can be assumed as laminar.

Governing Equations

The governing equations in the Cartesian coordinate system for forced, steady, laminar, three-dimensional, incompressible fluid flow and heat transfer in air, fin and flat tube subdomains are:

Air subdomain

Continuity:

$$\mathrm{div}\left(\rho_a \vec{\mathbf{u}}\right) = 0 \qquad (1)$$

Momentum:

$$\text{x...} \quad \mathrm{div}\left(\rho_a u \vec{\mathbf{u}}\right) = -\frac{\partial p}{\partial x} + \mathrm{div}\left(\mu_a \,\mathrm{grad}\, u\right) \qquad (2)$$

$$\text{y...} \quad \operatorname{div}\left(\rho_a v \vec{\mathbf{u}}\right) = -\frac{\partial p}{\partial y} + \operatorname{div}\left(\mu_a \operatorname{grad} v\right) \tag{3}$$

$$\text{z...} \quad \operatorname{div}\left(\rho_a w \vec{\mathbf{u}}\right) = -\frac{\partial p}{\partial z} + \operatorname{div}\left(\mu_a \operatorname{grad} w\right) \tag{4}$$

Energy:

$$\operatorname{div}\left(\rho_a \vec{\mathbf{u}} T_a\right) = \operatorname{div}\left(\frac{k_a}{c_a} \operatorname{grad} T_a\right) \tag{5}$$

Fin and flat tube subdomains

$$\operatorname{div}\left(\frac{k_{f,t}}{c_{f,t}} \operatorname{grad} T_{f,t}\right) = 0 \tag{6}$$

Fins and flat tubes are made of aluminium and eq. (6) comprises the same physical properties for either domain.

Boundary Conditions

Boundary conditions are:

The air inlet boundary:

$$u_a = u_{a,in} = \text{const.},\ v_a = 0,\ w_a = 0 \tag{7}$$

$$T_a = T_{a,in} = \text{const.} \tag{8}$$

The air outlet boundary:

$$\frac{\partial u_a}{\partial x} = 0, \frac{\partial v_a}{\partial x} = 0, \frac{\partial w_a}{\partial x} = 0, \frac{\partial T_a}{\partial x} = 0 \tag{9}$$

Air symmetry at the left and right boundaries:

$$\frac{\partial u_a}{\partial y} = 0, v_a = 0, \frac{\partial w_a}{\partial y} = 0, \frac{\partial T_a}{\partial y} = 0 \tag{10}$$

Flat tube surface on the refrigerant side:

$$T_{mc} = \text{const.} \tag{11}$$

Flat tube symmetry at the left and right boundaries:

$$\frac{\partial T_t}{\partial y} = 0 \tag{12}$$

Air symmetry at the upper and lower boundaries:

$$\frac{\partial u_a}{\partial z} = 0, \frac{\partial v_a}{\partial z} = 0, w_a = 0, \frac{\partial T_a}{\partial z} = 0 \tag{13}$$

Fin symmetry at the upper and lower boundaries:

$$\frac{\partial T_f}{\partial z} = 0 \tag{14}$$

Air – fin and air – flat tube interface respectively:

$$k_a \frac{\partial T_a}{\partial n} = k_f \frac{\partial T_f}{\partial n}, k_a \frac{\partial T_a}{\partial n} = k_t \frac{\partial T_t}{\partial n} \tag{15}$$

Numerical Treatment

The governing differential equations were discretized using the finite-volume method, fully described by Versteeg and Malalasekera [14] and Patankar [15], on a hybrid grid. The domain has been meshed using ANSYS Mesher and has been partly shown in Figure 2.

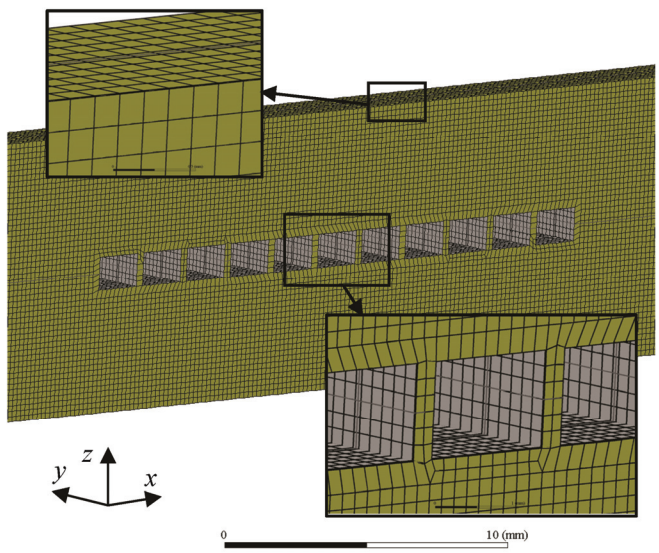

Figure 2 Grid system

Heat transfer and fluid flow simulations were performed using fluid flow and a heat transfer solver FLUENT, which uses the preceding set of equations for fluid flow and heat transfer conditions. The fluid is assumed to be incompressible with constant property values and the flow is assumed to be laminar. The SIMPLE algorithm for pressure–velocity coupling was used to ensure mass conservation and to obtain a pressure field. The convection–diffusion terms have been discretized using the Second-Order Upwind Scheme. Convergence criteria for momentum and energy were set to 10^{-6} and for continuity to 10^{-3}.

VALIDATION

The comparison of experimental and numerical data has been done in order to validate used numerical simulation.

The experimental measurements have been done in an open circuit wind tunnel that was used to prepare air and bring it towards the measuring zone. The main components of the

system were the air supply unit with a centrifugal fan, measuring orifice, heat exchanger with microchannel coil, instrumentation and data acquisition system. The experimental facility, data acquisition, and test heat exchanger details, followed with measurement conditions and results can be found in [10].

Numerical calculations have been performed for different flat tube surface temperatures (T_{mc}) and numerically obtained air outlet temperatures have been compared with experimentally acquired results (Figure 3).

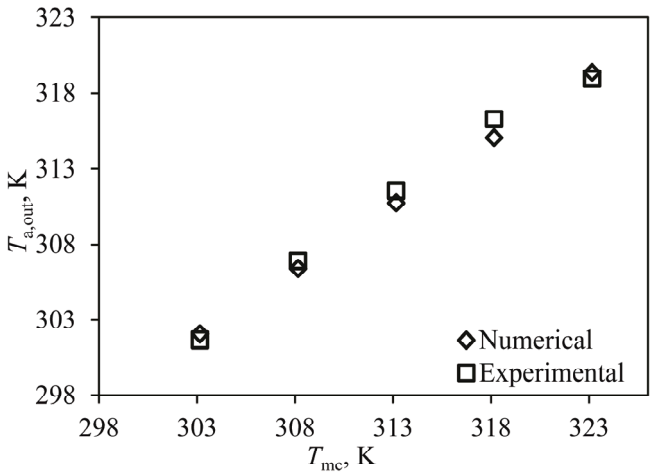

Figure 3 Numerically obtained air outlet temperatures compared to experimental results (test conditions: $T_{a,in}$ = 295.15 K, $u_{a,in}$ = 1.58 m s^{-1})

It can be seen that numerical simulation results coincide well with the experimental data and that deviations are within an acceptable range. Temperature differences are smaller than ±0.7 K, what can be taken as an assertion of used numerical simulation validity. Therefore, it can be concluded that the described mathematical model and numerical calculations can be used for the analysis of heat transfer heat exchanger with microchannel coil.

A QUEST FOR THE OPTIMAL DESIGN

The Box-Bhenken experimental design with three independent variables constrained to only three levels (minimum, medium and maximum) has been used. In this way, the total number of needed design points has been reduced to 15 among which the referent model has been used three times. The reduction of design points implemented this way saves a large amount of needed time, especially when compared with the full factorial design of the experiment (27 different design points).

Optimization Settings

For the optimization process, two geometry parameters and one operating condition have been chosen. Fin pitch (x_1), transversal MCHX tube row pitch (x_2) and inlet air velocity (x_3) have been selected as input parameters. All selected input parameters have been ranged in three equally spaced values: lowest, highest and the referent value. The referent values for each input parameter has been placed in the middle of the domain. All parameters have been normalised using the following expression:

$$X_i = \frac{2\left(x_i - x_{i,\mathrm{ref}}\right)}{x_{i,\max} - x_{i,\min}} \tag{16}$$

Table 2 shows uncoded and Table 3 shows coded values for selected input parameters.

Table 2 Ranges of uncoded selected input parameters

	Uncoded			
F_p	x_1, mm	1	1.5	2
P_t	x_2, mm	10	15	20
$u_{a,in}$	x_3, m s^{-1}	0.5	1	1.5

Table 3 Ranges of coded selected input parameters

	Coded			
F_p	X_1, /	-1	0	1
P_t	X_2, /	-1	0	1
$u_{a,in}$	X_3, /	-1	0	1

The working parameter setup has been done with following velocities and temperatures: air inlet velocities ($u_{a,in}$) varied from 0.5 to 1.5 m s^{-1}, air inlet temperature ($T_{a,in}$) was 283.15 K and flat tube surface temperature on the refrigerant side was 313.15 K.

The previously described mathematical model has been solved numerically for each set of prescribed design points. A total of 13 numerical simulations have been conducted. The heat transfer rate for one flat tube and one fin (Q_{mc}) has been calculated using FLUENT solver. Appropriate heat exchanger mass has been derived from the created 3D geometry model.

Definition of the Objective Function

To optimise heat exchanger power density according to three selected input parameters, a function that incorporates heat transfer rate and mass of the heat exchanger (power density) is formulated as follows:

$$f(x_1, x_2, x_3) = \frac{Q_{mc} / m_{mc}}{Q_{mc,ref} / m_{mc,ref}} \tag{17}$$

The developed objective function includes two variable parameters: power density (Q_{mc}/m_{mc}) for each prescribed design point compared to the power density of the referent model ($Q_{mc,ref}/m_{mc,ref}$). To increase the power density of MCHX this function should be maximised.

Power densities and eq. (17) results are given in Table 4 for a full set of selected input parameters (uncoded).

Table 4 Prescribed set of selected input parameters (uncoded), power densities and eq. (17) results

No.	x_1 mm	x_2 mm	x_3 m s^{-1}	Power density W kg^{-1}	$f(x_1,x_2,x_3)$
1	1	15	0.5	2065	0.52
2	1	10	1	3457	0.86
3	1.5	10	1.5	4229	1.06
4*	1.5	15	1	4007	1.00
5	2	10	1	2926	0.73
6	1	15	1.5	5404	1.35
7	2	20	1	4081	1.02
8*	1.5	15	1	4007	1.00
9	1.5	10	0.5	2043	0.51
10	2	15	1.5	4322	1.08
11	1	20	1	4141	1.03
12	1.5	20	0.5	2678	0.67
13	1.5	20	1.5	5365	1.34
14*	1.5	15	1	4007	1.00
15	2	15	0.5	2429	0.61

*referent values

The coefficients of the quadratic models for the equation (17) were acquired by a Gauss-Newton method and regression equation for selected input parameters (coded) has been generated:

$$\begin{aligned} f(x_1,x_2,x_3) = {} & 1-0.04083\cdot X_1+0.11264\cdot X_2+0.31524\cdot X_3 \\ & -0.04742\cdot X_1\cdot X_1 -0.04144\cdot X_2\cdot X_2-0.06542\cdot X_3\cdot X_3 \quad (18) \\ & +0.02939\cdot X_1\cdot X_2-0.09026\cdot X_1\cdot X_3+0.03127\cdot X_2\cdot X_3 \end{aligned}$$

The coefficient of determination for eq. (18) is R^2 = 99.88%. This proves that the proportion of the variance in the dependent variable that is predictable from the independent variables is valid and that it can be used in the following analysis.

Response Surfaces

Response surface plot for developed objective function eq. (17) has been shown in Figure 4. Fin pitch (x_1) and transversal tube row pitch (x_2) influence on power density have been explored. Air inlet velocity (x_3) has been set to its referent value.

In order to facilitate the assessment of the impact of the selected parameters on power density, the objective function gives a difference of heat exchanger power density compared to the referent heat exchanger.

From Figure 4 it can be seen that at lower values of transversal tube row pitch, obtained power densities are always lower than ones obtained for referent values. In case when x_2 is set at a medium level (referent value), power density rises. To obtain the highest power densities with inlet air velocities set at 1 m s^{-1} transversal tube row pitch should be set at range maximum limits.

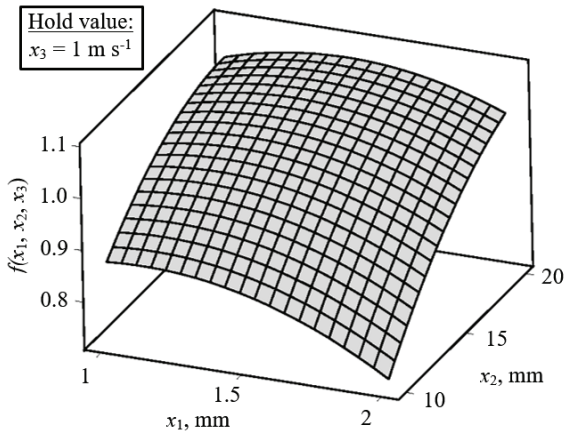

Figure 4 Response surface plot for objective function dependence on fin pitch (x_1) and tube row pitch (x_2). Hold value x_3 = 1 m s^{-1}

Although differences are relatively small, it can be seen that in the case when x_2 is close to 20 mm, surface plot points for fin pitch value around 1.5 mm to obtain the highest power density.

An additional simulation point has been created and numerically solved according to the best selection of input parameters pointed at Figure 4: x_1= 1.5 mm, x_2 = 20 mm and x_3 = 1 m s^{-1}. In the best selection of geometry input parameters with x_3 set at reference value power density gets 8.1% better than for referent values. Calculated power density for created simulation is 4330 W kg^{-1} and objective function value, eq.(17) equals 1.08.

Figure 5 gives the response surface plot for the same objective function and the same geometry parameters. The difference from Figure 4 is that the inlet air velocity is set at a range maximum level (x_3 = 1.5 m s^{-1}).

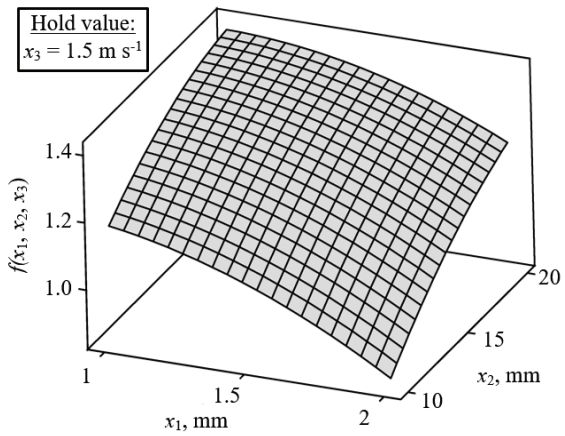

Figure 5 Response surface plot for objective function dependence on fin pitch (x_1) and tube row pitch (x_2). Hold value x_3 = 1.5 m s^{-1}

Higher inlet air velocity results with a higher mass flux of air. Consequently, heat transfer rate and appropriate power density become higher.

Another simulation point has been created and numerically solved for the best selection of input parameters pointed at Figure 5: x_1= 1 mm, x_2 = 20 mm and x_3 = 1.5 m s^{-1}. In the best selection of geometry input parameters, value power density gets 41% better than for referent values. Calculated power density for created simulation is 5637 W kg^{-1} and objective function value, eq.(17) equals 1.41.

In the case of selected input parameter $\boldsymbol{x_1}$ at the minimum and $\boldsymbol{x_2}$ at the maximum level, the power density of the heat exchanger becomes 41% better than for the referent values.

Optimisation by Genetic Algorithm

Nonlinear regression model shown in eq. (18) has been subjected to optimization by mean of genetic algorithm. Genetic algorithms are a type of optimization algorithm, aimed to find the optimal solution(s) to a given computational problem that maximizes or minimizes a particular function. Genetic algorithms represent one branch of the study field called evolutionary computation because they imitate the biological processes of reproduction and natural selection to solve for the `fittest' solutions [16]. The optimization has been carried out with the following parameters: Convergence rate 10^{-4}, mutation rate 0.075, population size 100, random seed 0 and maximum time without improvement 30.

The results of optimization of three variables obtained with optimization by genetic algorithm showed values analogous to previously, by Response Surface Methodology, pointed values: x_1= 1 mm, x_2 = 20 mm and x_3 = 1.5 m s^{-1}. This can be taken as proof of applied optimization methods validity. The power density of heat exchanger with a microchannel coil with optimised input geometry and operating parameters becomes higher.

CONCLUSION

This paper presents heat transfer analysis and optimization procedure of heat exchanger with microchannel coil according to heat exchanger power density. A number of heat transfer simulations have been done. The 3D mathematical model has been created and solved using fluid flow and a heat transfer solver FLUENT. The Box-Bhenken experimental design with three independent variables has been utilized for the creation of the prescribed data set. Thirteen numerical simulations have been conducted and function that incorporates heat transfer rate and mass of heat exchanger has been formulated. Both response surface plots and optimization by genetic algorithm pointed to optimum values of selected input parameters for which obtained power density was more than 40% higher than in the setup with referent values.

ACKNOWLEDGMENT

This work has been supported in part by the Croatian Science Foundation under the project IP-2016-06-4095 and in part by the University of Rijeka under the project number 17.10.2.1.05.

REFERENCES

[1] Ribatski, G., and Da Silva, J.D., Microchannel Phase Change Transport Phenomena –8– Condensation in Microchannels, Elsevier, 2016, pp. 287-324.

[2] Kaltra Innovativtechnik, https://www.kaltra.com/, accessed on 7th of April, 2019.

[3] Climetal Heat Exchangers, http://climetal.com/, accessed on 7th of April, 2019.

[4] Foo, Z.H., Cheng, K.X., Goh, A.L., and Ooi, K.T., Single-phase convective heat transfer performance of wavy microchannels in macro geometry, *Applied Thermal Engineering,* Vol. 141, 2018, pp. 675-687.

[5] Mandel, R., Shooshtari, A., and Ohadi, M., A "2.5-D" modeling approach for single-phase flow and heat transfer in manifold microchannels, *International Journal of Heat and Mass Transfer*, Vol. 126, 2018, pp. 317-330.

[6] Ronshin, F., and Chinnov, E., Experimental characterization of two-phase flow patterns in a slit microchannel, *Experimental Thermal and Fluid Science*, Vol. 103, 2019, pp. 262-273.

[7] Kwon, B., Maniscalco, N.I., Jacobi, A.M., and King, W.P., High power density two-phase cooling in microchannel heat exchangers, *Applied Thermal Engineering*, Vol. 148, 2019, pp. 1271-1277.

[8] Garrity, P.T., Klausner, J.F., and Mei, R., Performance of Aluminum and Carbon Foams for Air Side Heat Transfer Augmentation, Journal of Heat Transfer, Vol. 132, 2010, pp. 1-9.

[9] Box, G.E.P., Behnken, D.W., Some New Three Level Designs for the Study of Quantitative Variables, *Technometrics,* Vol 2, 1960, pp. 455-475.

[10] Glazar, V., Trp, A., Lenic, K., Kirincic, M., Experimental Analysis of Air-Water Heat Exchanger with Microchannel Coil Exposed to Different Working Parameters, *ISES Conference Proceedings Database - EuroSun 2018*, 2018.

[11] Montgomery, D.C., Design and Analysis of Experiments, Wiley, 2012, p. 752.

[12] Glazar, V., Trp, A., Lenic, K., Torbarina, F., Numerical analysis of heat transfer in air-water heat exchanger with microchannel coil, *E3S Web of Conferences 95, 02004, ICPEME 2019*, 2019.

[13] Jiyuan Tu, Guan-Heng Yeoh and Chaoqun Liu, Computational Fluid Dynamics - A Practical Approach, Elsevier, 2019, pp. 255-290.

[14] Versteeg, H.K., Malalasekera, W., An Introduction to Computational Fluid Dynamics: The Finite Volume Method, Pearson, Prentice hall, 2007.

[15] Patankar, S. V., Numerical Heat Transfer and Fluid Flow, Hemisphere, New York, 1998.

[16] Haupt, R.L., Haupt, S.E., Practical Genetic Algorithms, Wiley-Interscience, New York, 2004.